Mecánica Computacional Vol. XXIV
A. Larreteguy (Editor)
Buenos Aires, Argentina, Noviembre 2005

NUMERICAL MODELLING OF THE CONCURRENT EFFECT OF SOLID DEFORMATION AND MELT FLOW ON HEAT AND SOLUTE TRANSFER IN BINARY ALLOYS, WITH APPLICATION TO THE SECONDARY COOLING STAGE OF STEEL SLABS CONTINUOUS CASTING

Victor D. Fachinotti[†*], Steven Le Corre[†] and Michel Bellet[†]

[†] Ecole des Mines de Paris
Centre de Mise en Forme des Matériaux (CEMEF)
UMR CNRS 7635, BP 207, F-06904 Sophia Antipolis, France

[*] Consejo Nacional de Investigaciones Científicas y Técnicas (CONICET)
Centro Internacional de Métodos Computacionales en Ingeniería (CIMEC)
Parque Tecnológico del Litoral Centro, Ruta Nacional 168, Paraje El Pozo
S3007ABA Santa Fe, Argentina

ABSTRACT

We introduce a thermo-mechanical and macrosegregation model that considers a solidifying alloy as a binary mixture made of a liquid and a solid phase. Macroscopic conservation laws for mass, momentum and solute are obtained by spatial averaging of the respective microscopic conservation equations. Assuming local thermal equilibrium, a single equation for the conservation of the mixture energy is then written. A single equation can be obtained for the solute as well by invoking a proper microsegregation rule. The numerical implementation in a 2D finite element code is then detailed. In order to validate the two-phase mechanical model, an academic problem is solved. Lastly, an industrial application for continuous casting of steel slabs is shown, where the ability of the formulation to describe the formation of central macrosegregation during the secondary cooling of slab continuous casting processes is enlightened.

1 INTRODUCTION

Macrosegregation, *i.e.* the lack of homogeneity of solute concentration at the whole scale of a solidified product, is a central problem since it strongly influences the further workability of the cast products and their mechanical properties. Macrosegregation is the result of slow

interdendritic flow of molten liquid and transport of alloying elements at the product scale. In most numerical models, only the natural convection induced by thermal and solutal gradients is taken into account. The influence of the solid kinetics on the fluid flow is rarely modelled. However, as summarized by Flemings,[1] the macrosegregation of chemical species may depend strongly on the deformation of the solid skeleton in the mushy zone. This is especially the case in continuous casting: as bulging occurs between the supporting rolls, there exists a large mushy zone which deforms together with the solid shell.

In the present study, the mushy zone is considered as an effective two-phase medium. On one hand, the solid material is considered as an incompressible viscoplastic material, obeying a constitutive equation of power-law type. Invoking homogenization results,[2] its macroscopic flow rule is viscoplastic, including compressibility, so that the solid continuum can be seen as a deformable compressible porous medium. On the other hand, the liquid phase is intrinsically Newtonian. At the macroscopic scale, its momentum interaction with the solid skeleton is described by the Darcy law of flow through a porous medium. The present contribution enters then the third family of models previously mentioned. In addition, the present formulation includes mass transfer between liquid and solid, and the couplings with heat transfer and solute transport is taken into account. The two-dimensional numerical implementation of the corresponding mass, momentum, energy and solute conservation equations has been carried out in the finite element software R2SOL, developed at CEMEF.

2 MACROSCOPIC BALANCE EQUATIONS RESTRICTED TO EACH PHASE

At the microscopic scale, inside each phase, the thermo-mechanical evolution is assumed to be governed by the usual mass, momentum, energy and solute balances. In this work, the balance equations for the mixture, at the (macroscopic) scale of a representative elementary volume (REV), are obtained using the spatial averaging method over a fixed control volume V_0. This method is classical and will not be detailed here (see[3–6] for further details on its basic principles).

Given any function ψ defined over the phase k, we can define

$$\text{the intrinsic average value:} \qquad \psi_k = \langle\psi\rangle^k = \frac{1}{V_k}\int_{V_0} \psi(\boldsymbol{x})\chi_k(\boldsymbol{x})\,\mathrm{d}V, \tag{1}$$

$$\text{the classic average value:} \qquad \langle\psi^k\rangle = \frac{1}{V_0}\int_{V_0} \psi(\boldsymbol{x})\chi_k(\boldsymbol{x})\,\mathrm{d}V, \tag{2}$$

where V_k denotes the volume occupied by phase k in the REV, and χ_k is the characteristic function of phase k ($= 1$ in phase k and 0 elsewhere). Both average values are related by

$$\langle\psi^k\rangle = g_k\psi_k. \tag{3}$$

where g_k is the volume fraction of phase k.

Now, let us consider the solidifying alloy in the mushy state as a saturated solid-liquid medium, such that $g_s + g_l = 1$.

The application of the spatial averaging process to microscopic balance equations in each phase k ($k = s, l$) yields the following set of macroscopic equations:

$$\text{Momentum:} \quad \nabla \cdot (g_k \boldsymbol{\sigma}_k) + \boldsymbol{M}_k + g_k \rho_k \boldsymbol{g} = \frac{\partial}{\partial t}(g_k \rho_k \boldsymbol{v}_k) + \nabla \cdot (g_k \rho_k \boldsymbol{v}_k \times \boldsymbol{v}_k), \tag{4}$$

$$\text{Mass:} \quad \frac{\partial}{\partial t}(g_k \rho_k) + \nabla \cdot (g_k \rho_k \boldsymbol{v}_k) = \Gamma_k, \tag{5}$$

$$\text{Energy:} \quad \frac{\partial}{\partial t}(g_k \rho_k h_k) + \nabla \cdot (g_k \rho_k h_k \boldsymbol{v}_k) + \nabla \cdot \langle \boldsymbol{q}^k \rangle = Q_k, \tag{6}$$

$$\text{Solute:} \quad \frac{\partial}{\partial t}(g_k w_k) + \nabla \cdot (g_k w_k \boldsymbol{v}_k) + \nabla \cdot \langle \boldsymbol{j}^k \rangle = J_k, \tag{7}$$

where ρ denotes the density, $\boldsymbol{v}$ the velocity field, $\boldsymbol{\sigma}$ the Cauchy stress tensor, $\boldsymbol{g}$ the gravity vector, h the enthalpy per unit mass, $\boldsymbol{q}$ the heat flow vector, w the solute concentration per unit volume, and $\boldsymbol{j}$ its flux. The terms Γ, $\boldsymbol{M}$, Q and J are associated with the exchanges of mass, momentum, energy and solute, respectively, between the two phases.

The following subsections will now detail the additional assumptions and constitutive models adopted in this paper for each variable appearing in those macroscopic balance equations.

2.1 Mass conservation

The local mass balance at the interface between phases ensures that $\Gamma_s + \Gamma_l = 0$.[6] Then, summing equations (5) for the liquid and solid phases, and assuming that the densities of the two phases remain constant (but not necessarily equal), we get after some trivial operations:

$$(1 - \Delta\varepsilon^{tr})\nabla \cdot (g_s \boldsymbol{v}_s) + \nabla \cdot (g_l \boldsymbol{v}_l) = \frac{\partial g_s}{\partial t}\Delta\varepsilon^{tr}, \tag{8}$$

where $\Delta\varepsilon^{tr} = (\rho_l - \rho_s)/\rho_l$ denotes the relative change of volume associated with solidification (often negative for metallic alloys).

2.2 Momentum conservation

The spatial averaging method used in this work is efficient to obtain in a simple way the macroscopic governing equations of the semi-solid alloy but does not enable to go further in the specifications of the macroscopic model. Reliable constitutive equations would require more sophisticated approaches such as homogenization[2,7] associated with numerical simulation at the microscopic scale, but this is not within the scope of this work. The full definition of the two-phase model will simply be based on further constitutive assumptions, consistent with previous theoretical works.

2.2.1 Macroscopic constitutive equation for the liquid phase

At the microscopic scale, we assume that the liquid metal behaves as an incompressible Newtonian fluid. The incompressibility hypothesis is valid as long as the temperature range of the

solidification interval remains narrow enough. In such a case, we can write:

$$\boldsymbol{s} = 2\mu_l \dot{\boldsymbol{\varepsilon}}(\boldsymbol{v}), \tag{9}$$

where $\boldsymbol{s} = \boldsymbol{\sigma} + p\boldsymbol{I}$ is the deviatoric part of the stress tensor $\boldsymbol{\sigma}$, $p = -\operatorname{tr}(\boldsymbol{\sigma})/3$ being the hydrostatic pressure, μ_l the viscosity of the liquid, and $\dot{\boldsymbol{\varepsilon}}(\boldsymbol{v}) = (\nabla \otimes \boldsymbol{v} + (\nabla \otimes \boldsymbol{v})^T)/2$ the strain rate tensor.

As suggested by Ganesan and Poirier[8] and Rappaz et al,[6] we adopt the following model for the macroscopic deviatoric stress tensor:

$$\boldsymbol{\Sigma}^l = \langle \boldsymbol{s}^l \rangle = 2\mu_l g_l \operatorname{dev}(\dot{\boldsymbol{\varepsilon}}(\boldsymbol{v}_l)). \tag{10}$$

where $\operatorname{dev}(*)$ denotes the deviatoric part of tensor $(*)$.

2.2.2 Macroscopic constitutive equation for the solid phase

Experimental studies on the behavior of metallic alloys at high temperature show that the response of the solid phase is well described by constitutive equations of the Norton-Hoff type.[9–11] Like the liquid, the solid is assumed to be incompressible at the microscopic scale, such that its response can be characterized at this scale by the following constitutive equation:

$$\boldsymbol{s} = 2K_s \left(\sqrt{3}\dot{\varepsilon}_{eq}\right)^{m-1} \dot{\boldsymbol{\varepsilon}}(\boldsymbol{v}), \tag{11}$$

where K_s and m denote the consistency and the strain rate sensitivity, respectively, and $\dot{\varepsilon}_{eq}$ the von Mises equivalent strain rate.

For solid fractions above the coherency fraction $g_{s_{cohe}}$, following the theoretical analysis of Geindreau and Auriault,[2] the effective stress tensor

$$\boldsymbol{\Sigma}^s = \langle \boldsymbol{s}^s \rangle - \langle p^s \rangle \boldsymbol{I} + g_s p_l \boldsymbol{I} \tag{12}$$

is expressed as a degree m homogeneous function with respect to the strain rate tensor $\langle \dot{\boldsymbol{\varepsilon}} \rangle^s = \dot{\boldsymbol{\varepsilon}}(\boldsymbol{v}^s)$. Note that such a result is valid for small values of, which is generally the case for the solidification problems under consideration in this work. Then, the solid phase can be modelled as a compressible power-law fluid. We therefore adopt the compressible viscoplastic constitutive model:[9,12,13]

$$\boldsymbol{\Sigma}^s = 3K_s \left(\sqrt{3}\langle \dot{\boldsymbol{\varepsilon}} \rangle^s_{eq}\right)^{m-1} \left(\frac{1}{A}\langle \dot{\boldsymbol{\varepsilon}} \rangle^s + \left(\frac{1}{9B} - \frac{1}{3A}\right) \operatorname{tr}\left(\langle \dot{\boldsymbol{\varepsilon}} \rangle^s\right) \boldsymbol{I}\right), \tag{13}$$

where A and B are rheological functions that depend on the solid volume fraction and for which several models can be found.[9,12,14,15] The constitutive equations of the solid phase at the macroscopic scale then take the form

For lower solid fractions, i.e. below $g_{s_{cohe}}$, the solid phase will be supposed to be stress-free, which is an admissible hypothesis for modelling the sedimentation of free solid grains in the liquid pool (as in globulitic solidification[16]).

2.2.3 Exchange of momentum

According to Ni and Beckermann,[4] $\boldsymbol{M}_k$ can be partitioned as:

$$\boldsymbol{M}_k = \boldsymbol{M}_k^d + \boldsymbol{M}_k^p, \tag{14}$$

the first part being the contribution of deviatoric stresses and the second one the contribution of the isotropic part, and it can easily be shown that

$$\boldsymbol{M}_s^d + \boldsymbol{M}_l^d = \boldsymbol{0} \quad \text{and} \quad \boldsymbol{M}_s^p + \boldsymbol{M}_l^p = \boldsymbol{0}. \tag{15}$$

The liquid being a Newtonian incompressible fluid with a very low viscosity, we will assume that the pressure equilibrium in the liquid phase is almost instantaneous. Subsequently, the interfacial pressures[4] in both phases (p_k^*) equal the intrinsic average value of liquid pressure, *i.e.* its microscopic value:

$$p_l^* = p_s^* = p_l. \tag{16}$$

Therefore, $\boldsymbol{M}_k^p$ can be expressed as follows:[4]

$$\boldsymbol{M}_s^p = -\boldsymbol{M}_l^p = -p_l \nabla g_l = p_l \nabla g_s. \tag{17}$$

On the other hand, for $g_s < g_{s_{coh e}}$, the dissipative term $\boldsymbol{M}_k^d$ represents the filtration force exerted by the liquid flowing through the solid, assumed to behave as a rigid porous medium,[2,6] and is expressed as:

$$\boldsymbol{M}_s^d = -\boldsymbol{M}_l^d = \frac{g_l^2 \mu_l}{\kappa}(\boldsymbol{v}_l - \boldsymbol{v}_s). \tag{18}$$

being κ the permeability of the solid matrix in the mushy zone, assumed to be isotropic, defined by the Carman-Kozeny formula

$$\kappa = \frac{\lambda_2^2 g_l^3}{180 g_s^2}, \tag{19}$$

where λ_2 is the secondary dendrite arms spacing.

2.2.4 Final macroscopic momentum balance equations in solid and liquid

Considering the above assumptions, we obtain the following momentum balance equations for the solid phase:

$$\nabla \cdot \boldsymbol{\Sigma}^s - g_s \nabla p_l + \frac{g_l^2 \mu_l}{\kappa}(\boldsymbol{v}_l - \boldsymbol{v}_s) + g_s \rho_s \boldsymbol{g} = \rho_s \frac{\partial}{\partial t}(g_s \boldsymbol{v}_s) + \rho_s \nabla \cdot (g_s \boldsymbol{v}_s \times \boldsymbol{v}_s), \tag{20}$$

and the liquid phase:

$$\nabla \cdot \boldsymbol{\Sigma}^l - g_l \nabla p_l - \frac{g_l^2 \mu_l}{\kappa}(\boldsymbol{v}_l - \boldsymbol{v}_s) + g_l \rho_l \boldsymbol{g} = \rho_l \frac{\partial}{\partial t}(g_l \boldsymbol{v}_l) + \rho_l \nabla \cdot (g_l \boldsymbol{v}_l \times \boldsymbol{v}_l). \tag{21}$$

Above equations are subject to the following boundary conditions:

$$\boldsymbol{v}_s = \boldsymbol{v}_l = \boldsymbol{v}_{imp} \qquad \text{on } \partial\Omega_u, \tag{22}$$

$$\langle \boldsymbol{\sigma}^s \rangle \boldsymbol{n} = \langle \boldsymbol{\sigma}^l \rangle \boldsymbol{n} = \boldsymbol{T}_{imp}, \qquad \text{on } \partial\Omega_s, \tag{23}$$

where $\langle \boldsymbol{\sigma}^s \rangle = \boldsymbol{\Sigma}^s - g_s p_l \boldsymbol{I}$, $\boldsymbol{v}_{imp}$ and $\boldsymbol{T}_{imp}$ are the imposed surface velocity and traction on the non-overlapped portions $\partial\Omega_u$ and $\partial\Omega_s$ of the boundary $\partial\Omega$ of the analysis domain Ω; $\boldsymbol{n}$ is the normal unit vector pointing outwards $\partial\Omega$.

2.3 Energy conservation

At the microscopic level, heat flux is described by the Fourier law:

$$\boldsymbol{q} = -\lambda \nabla T. \tag{24}$$

where T is the temperature and λ the thermal conductivity.

Further, local thermal equilibrium is assumed, such that:

$$T_s = T_l = T. \tag{25}$$

The enthalpies of both phases can then be written as a function of the temperature T as follows:

$$h_s = \int_{T_0}^{T} c_p(\tau)\, \mathrm{d}\tau \quad \text{and} \quad h_l = h_s + L, \tag{26}$$

where c_p and L are the heat capacity and latent heat per unit mass, respectively. The average mixture enthalpy per unit mass takes the form

$$\langle h \rangle = f_s h_s + f_l h_l = \int_{T_0}^{T} c_p(\tau)\, \mathrm{d}\tau + f_l L, \tag{27}$$

where f_k is the mass fraction of phase k, defined as $f_k = \rho_k g_k / \langle \rho \rangle$, $\langle \rho \rangle = g_s \rho_s + g_l \rho_l$ being the average density of the solid-liquid mixture.

By invoking hypothesis (25), the energy conservation is written as a single equation which is the sum of the energy balance on both phases, where the terms of exchange Q_s and Q_l cancel themselves. After elementary calculations, we obtain the following advection-diffusion equation for the average mixture enthalpy:

$$\langle \rho \rangle \frac{\partial \langle h \rangle}{\partial t} + \langle \rho \boldsymbol{v} \rangle \cdot \nabla \langle h \rangle - \nabla \cdot (\tilde{\kappa} \nabla \langle h \rangle) + S_T = 0, \tag{28}$$

being

$$\langle \rho \boldsymbol{v} \rangle = g_s \rho_s \boldsymbol{v}_s + g_l \rho_l \boldsymbol{v}_l, \tag{29}$$

$$\tilde{\kappa} = \langle \lambda \rangle \frac{\partial T}{\partial \langle h \rangle}, \tag{30}$$

$$S_T = L \nabla \cdot \left(\langle \rho \rangle (\boldsymbol{v}_l - \boldsymbol{v}_s) f_s f_l \right), \tag{31}$$

where $\langle \lambda \rangle = g_s \lambda_s + g_l \lambda_l$ is the average conductivity of the mixture.

The heat balance equation (28) is subject to the initial condition:

$$T = T_0 \qquad \text{at } t = 0 \text{ in } \Omega, \tag{32}$$

and the following boundary conditions :

$$T = T_w \qquad \text{at } t > 0 \text{ on } \partial\Omega_T, \tag{33}$$

$$(-\langle \lambda \rangle \nabla T) \cdot \boldsymbol{n} = q_w \qquad \text{at } t > 0 \text{ on } \partial\Omega_q, \tag{34}$$

$$(-\langle \lambda \rangle \nabla T) \cdot \boldsymbol{n} = h(T - T_{ext}) \qquad \text{at } t > 0 \text{ on } \partial\Omega_c, \tag{35}$$

prescribing the temperature T_w on $\partial\Omega_T$, the heat flux q_w through $\partial\Omega_q$, and the heat exchange through $\partial\Omega_c$ due to convection to the environment at temperature T_{ext} with h as the convection coefficient; $\partial\Omega_T$, $\partial\Omega_q$, and $\partial\Omega_c$ are non-overlapping portions of the boundary $\partial\Omega$ of Ω, being $\boldsymbol{n}$ the unit normal vector pointing outwards to $\partial\Omega$.

2.4 Solute conservation

The solute flux vector $\boldsymbol{j}$ is determined at the microscopic scale by the first law of Fick, which can be written for the isotropic case as follows:

$$\boldsymbol{j} = -D \nabla w, \tag{36}$$

being D the solute diffusion coefficient. By summing the solute conservation equations averaged for each phase, and considering that $J_s = -J_l$, we obtain:

$$\frac{\partial \langle w \rangle}{\partial t} + \nabla \cdot \langle w \boldsymbol{v} \rangle + \nabla \cdot \langle \boldsymbol{j} \rangle = 0, \tag{37}$$

where

$$\langle w \rangle = \langle w^s \rangle + \langle w^l \rangle = g_s w_s + g_l w_l, \tag{38}$$

$$\langle w \boldsymbol{v} \rangle = \langle (w \boldsymbol{v})^s \rangle + \langle (w \boldsymbol{v})^l \rangle = g_s w_s \boldsymbol{v}_s + g_l w_l \boldsymbol{v}_l, \tag{39}$$

$$\langle \boldsymbol{j} \rangle = \langle \boldsymbol{j}^s \rangle + \langle \boldsymbol{j}^l \rangle = -\langle (D \nabla w)^s \rangle - \langle (D \nabla w)^l \rangle = -g_s D_s \nabla w_s - g_l D_l \nabla w_l. \tag{40}$$

The diffusion coefficients D_k are very small (particularly D_s), so that they are usually neglected. However, in this work we neglect the diffusion in the solid phase, but maintain the diffusion in the liquid phase since it has a stabilizing effect on the numerical solution. Then:

$$\langle \boldsymbol{j} \rangle \approx -g_l D_l \nabla w_l. \tag{41}$$

Now, we assume the perfect diffusion of solute in the solid and the liquid phase at the microscopic scale. This is the lever rule for microsegregation, which allows us to write

$$w_l = \frac{T - T_m}{m_l}, \tag{42}$$

$$w_s = k w_l, \tag{43}$$

$$\langle w \rangle = (g_l + k g_s) w_l. \tag{44}$$

where T_m is the melting temperature of the pure substance and m_l the slope of the liquidus line, and k is the partition coefficient (equal to the ratio between the slopes of the liquidus and solidus lines). The above equations imply the additional assumption of straight solidus and liquidus lines in the equilibrium phase diagram.

Then, we can write the solute balance equation in the form of an advection-diffusion equation for the average concentration, as follows:

$$\frac{\partial \langle w \rangle}{\partial t} + \boldsymbol{v}^w \cdot \nabla \langle w \rangle - \nabla \cdot \left(\tilde{D} \nabla \langle w \rangle \right) + S_w = 0, \tag{45}$$

being

$$\boldsymbol{v}^w = \boldsymbol{v}_s + \frac{g_l}{g_l + k g_s} (\boldsymbol{v}_l - \boldsymbol{v}_s), \tag{46}$$

$$\tilde{D} = \frac{g_l}{g_l + k g_s} D_l, \tag{47}$$

$$S_w = \langle w \rangle \nabla \cdot \boldsymbol{v}_s + w_l \nabla \cdot \left(g_l (\boldsymbol{v}_l - \boldsymbol{v}_s) \right). \tag{48}$$

Equation (45) is subject to the initial condition

$$\langle w \rangle = w_0 \qquad \text{at } t = 0 \text{ in } \Omega, \tag{49}$$

being w_0 the initial solute distribution, usually equal to the nominal solute content of the alloy.

Further, we assume that there is no solute flux through the domain boundary, *i.e.*:

$$\nabla \langle w \rangle \cdot \boldsymbol{n} = 0 \qquad \text{at } t > 0 \text{ on } \partial\Omega. \tag{50}$$

3 NUMERICAL IMPLEMENTATION

This formulation was implemented in the two-dimensional code R2SOL for finite element analysis. A detailed explanation can be found in an authors' previous work,[17] so that just a brief description will be included in this paper.

First, all the balance equations are integrated in time using an implicit two-points scheme.

The momentum balance in solid and liquid phase, equations (20) and (21) respectively, were solved using mixed pressure-velocity $P1^+/P1$ triangular finite elements.[18] As both equation are strongly coupled, they are solved simultaneously, together with the momentum equation (8) that serves as closure equation.

The different kinematics of solid and liquid phases are dealt with by means of the Arbitrary Lagrangian-Eulerian (ALE) method proposed by Bellet and Fachinotti.[19]

On the other hand, both thermal and macrosegregation problems, which are governed by similar advection-diffusion equations, are solved using linear triangular ($P1$) finite elements, formulated using the Streamline-Upwind Petrov/Galekin (SUPG) method.[20]

3.1 Thermo-macrosegregation coupling: the "microsegregation box"

Thermal and macrosegregation solutions interacts due to the simultaneous influence of both enthalpy and solute concentration on the local liquid or solid fraction. Assuming $\langle h\rangle$ and $\langle w\rangle$ to be known from the solution of thermal and macrosegregation problems, respectively, we invoke the enthalpy dependency on g_l and T defined by equation (27), the relationship (42) between w_l and T derived from the equilibrium phase diagram, and the microsegregation rule (44) relating relationship $\langle w\rangle$ to w_l and g_l, in order to pose a system of scalar equations from which w_l, g_l and T can be computed. The so-defined "microsegregation box" can be expressed as follows:

$$\boldsymbol{m}(w_l, T, g_l; \langle h\rangle, \langle w\rangle) = \begin{bmatrix} \langle h\rangle - \int_{T_0}^{T} c_p(\tau)\,\mathrm{d}\tau - g_l L \\ T - T_m - m_l w_l \\ \langle w\rangle - (g_l + k g_s) w_l \end{bmatrix} = \boldsymbol{0}. \tag{51}$$

Henceforth, by writing $(*;\bullet)$, it is implied that $(*)$ are variables and $(\bullet)$ are parameters.

This system has a closed analytical solution only if the heat capacity c_p is assumed to be constant. Otherwise, it is solved numerically using a regula-falsi method, spanning between $g_l = 0$ at the solidus temperature T_{sol} (or $g_l = g_{l_{eut}}$ at the beginning of the eutectic transformation at temperature T_{eut}) and $g_l = 1$ at the liquidus temperature T_{liq}. This algorithm serves also for the computation of $\partial T/\partial\langle h\rangle$.

Let us remark that the system (51), containing three scalar unknowns, has to be solved locally for each sampling point of the mesh at each step of the iterative solution of the thermal and macrosegregation problems.

3.2 Global coupling scheme

Besides the interaction between them, thermal and macrosegregation models are also coupled to the mechanical model. On the one hand, mechanical properties are in general dependent on temperature, and temperature and solute gradients induce natural convection. On the other hand, the velocities computed from the mechanical analysis define the advection velocities $\tilde{\boldsymbol{v}}$ and $\tilde{\boldsymbol{v}}^w$ in the energy and solute balance equations, respectively.

The coupled solution of all the balance equations is achieved using a simple staggered scheme, where these equations are solved successively at each time step, as described as follows:

- **New time instant** $t \leftarrow t + \Delta t$:

– **Initialization**:

$$k = 0,$$
$$(\boldsymbol{v}_s, \boldsymbol{v}_l, p_l, \langle h\rangle, \langle w\rangle; T, w_l, g_l)^{(0)}_{t+\Delta t} = (\boldsymbol{v}_s, \boldsymbol{v}_l, p_l, \langle h\rangle, \langle w\rangle; T, w_l, g_l)_t$$

– **New coupling iteration** $k \leftarrow k+1$:

1) Obtain $\langle h\rangle^{(k)}$ by solving the *thermal problem*.
2) Obtain $\langle w\rangle^{(k)}$ by solving the *macrosegregation problem*.
3) Obtain $w_l^{(k)}$, $T^{(k)}$, and $g_l^{(k)}$ by calling the *"microsegregation box"*.
4) Obtain $\boldsymbol{v}_s^{(k)}$, $\boldsymbol{v}_l^{(k)}$, and $p_l^{(k)}$ by solving the *mechanical problem*.
5) *Check convergence*:
   * If $\|(*)^{(k)} - (*)^{(k-1)}\| >$tolerance, go to the next coupling iteration.
   * Otherwise, update the variables

$$(\boldsymbol{v}_s, \boldsymbol{v}_l, p_l, \langle h\rangle, \langle w\rangle; T, w_l, g_l)_{t+\Delta t} = (\boldsymbol{v}_s, \boldsymbol{v}_l, p_l, \langle h\rangle, \langle w\rangle; T, w_l, g_l)^{(k)}_{t+\Delta t}$$

Then, go to the next time step.

In the convergence checking, $(*)$ represents any or some of the involved variables. However, in this work the time step is assumed to be small enough, and only one coupling iteration per time step is performed, making that checking superfluous.

4 APPLICATION

Let us consider a steel slab continuous casting process. The cast material consists of the 18M5Nb steel from ARCELOR, modelled as a binary iron-carbon alloy, with a nominal carbon content of 0.18%. Material and process data correspond to this steel as produced by ARCELOR, and will not be given here. The casting velocity V_{cast} is set to 0.86 m/min.

The hypothesis of coherent solid phase obliges us to start the two-phase analysis at a transverse section, say the initial two-phase section, far enough from the meniscus.

Up to this two-phase section, located 11. m-far from the meniscus in this case, a classical "one-phase" thermo-mechanical analysis[22,23] is performed.

In Figure 1 we observe thermal results from the "one-phase" analysis, particularly concerning the liquid fraction distribution along the strand. The enthalpy distribution at the initial two-phase section serves as initial condition for the two-phase thermal analysis.

Since the current version of the "one-phase" macrosegregation solver[24] is not able up to date to work under continuous casting conditions, we will assume a uniform solute concentration w_0 (equal to the nominal carbon content) in the initial two-phase section as initial condition. Although it implies an important simplification, this hypothesis let us distinguish the effect of solid deformation from the other sources of macrosegregation that are relevant in the earlier

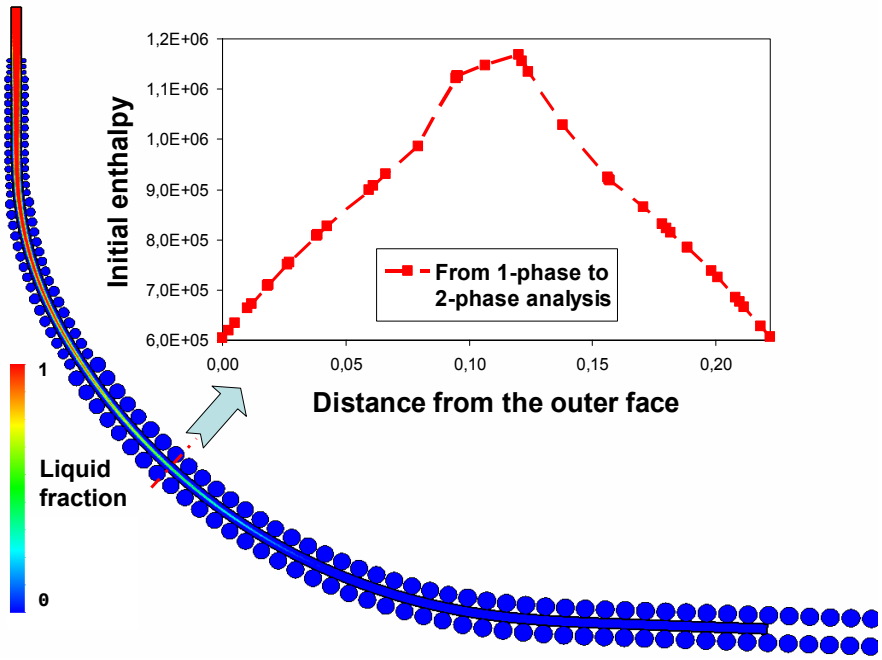

Figure 1: One-phase analysis of steel continuous casting process. On the left, distribution of liquid fraction along the slab. On the top, the enthalpy distribution at the initial two-phase section serving as initial thermal condition for the two-phase analysis.

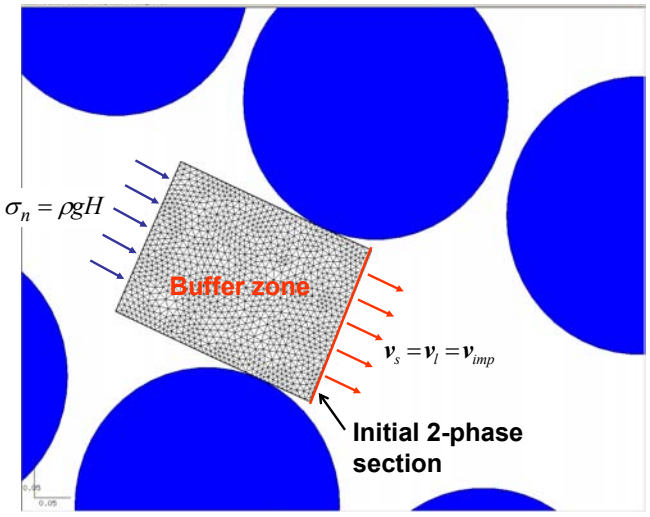

Figure 2: Two-phase analysis of steel continuous casting process: finite element mesh for the buffer zone and mechanical boundary conditions.

stages of the continuous casting process (for instance, macrosegregation by natural convection driven by thermal and solutal gradients).

In order to use the global unsteady-state approach,[22,23] a buffer zone is defined, consisting of a thick slice of the slab that ends at the initial two-phase section, as shown in Figure 2. Unlike in the one-phase analysis, where the buffer zone is a fictitious right cylindrical slice located above the meniscus, the buffer zone now lies in the curved portion of the caster. As before, the buffer length must be greater than the maximum displacement per time step of any particle in the initial two-phase section, otherwise it could be impossible to find the particle antecedent in the advection calculations.

The domain of analysis will increase as the strand moves down the caster, from its initial configuration coincident with the buffer zone to the whole domain we are interested in. In this case, the final domain extends up to a section located at a casting distance of 3.25 m, as shown in Figure 3, where the analysis stops after exceeding the maximum number of finite elements admitted by the current version of R2SOL (80000).

The solid phase assumed to be coherent all along the analysis, we assume that the mesh evolves with a velocity equal to the intrinsic solid velocity. In such a way, the mesh become rarely degenerated, with the consequent saving of the computational time associated to re-meshing.

In the buffer zone, the enthalpy and solute distributions are assumed not to vary in the longitudinal (i.e. casting) direction, remaining equal to those of the initial two-phase section.

Concerning the mechanical analysis, the metallostatic pressure is applied to the upper face of the buffer zone (H in Figure 2 denotes the metallostatic head), while at the current lower face a fictitious extracting tool is modelled by imposing an uniform velocity $\boldsymbol{v}_{imp}$ in the axis direction, with $\|\boldsymbol{v}_{imp}\| = V_{cast}S/S_0$, being S_0 the area of the meniscus section and S the current lower face area.

The two-phase analysis stops at a casting distance of 3.25 m, as shown in Figure 3, after exceeding the maximum number of finite elements admitted by the current version of R2SOL (80000). This figure also plots on the right top the initial liquid fraction, making apparent an important problem concerning the coupling of one-phase and two-phase models. The one-phase model used for initialize the two-phase analysis[22] is mainly devoted to the thermo-mechanical analysis in the solidified shell, the mushy and liquid zones being treated in an approximative way, with rather few elements. Due to the huge computational time and memory requirements, it is nowadays unfeasible to perform a one-phase analysis up to the initial two-phase section with a mushy zone as refined as needed for the two-phase analysis. This problem is open and should be the matter of future developments.

Regarding macrosegregation, the final carbon segregation $\langle w \rangle - w_0$ is depicted in Figure 4. We observe there the ability of the current model to capture the phenomenon of central (positive) segregation, characteristic of continuously cast steel slabs.[25]

Even if the solidification is not completed so that the solute concentrations can still evolve, the computed level of macrosegregation seems to be significantly lower than in reality. Nevertheless, we feel that this could be strongly improved by the use of more realistic constitutive

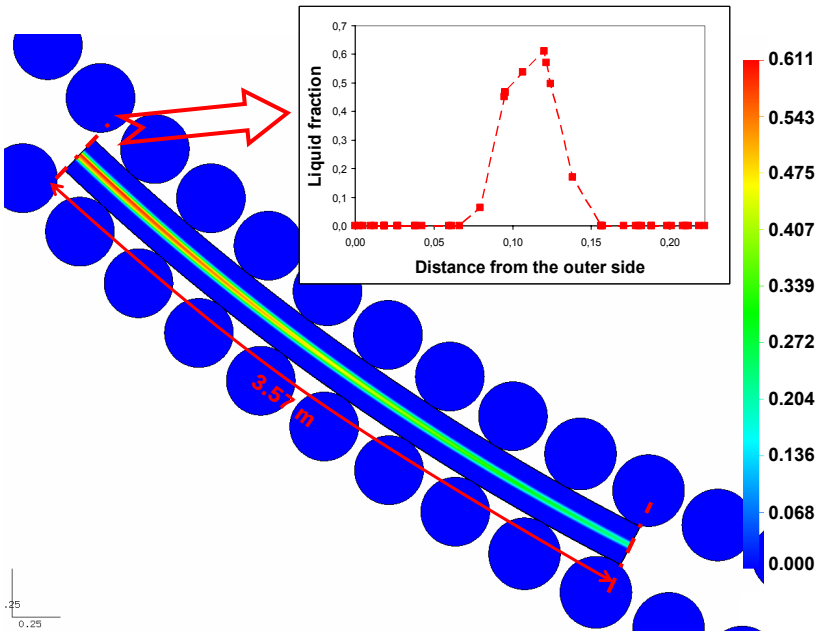

Figure 3: Final distribution of liquid fraction in the analyzed portion of the slab.

models and parameters, especially for the solid phase compressible behavior and the mechanical interaction term. Furthermore, as already mentioned, a finer mesh would be necessary to confirm such trends.

5 CONCLUSIONS AND PERSPECTIVES

This work contributes to the understanding of the complex phenomena observed in a solidifying medium, particularly in the late stages of solidification once the solid phase has already developed a coherent structure. This assumption was thought to be adequate to characterize the secondary cooling region of continuous casting processes, when the cast strand is subject to the alternate effects of rolling and bulging, which induces alternate compression and expansion states in the mushy core of the strand. The solid skeleton in the mushy region is looked as a viscoplastic compressible body and can be assimilated to a sponge that absorbs or expels the interstitial liquid, rich in segregated solutes. This mechanism is the main source of macrosegregation in the secondary cooling zone, and its responsibility on central macrosegregation in continuously cast steel slab has been demonstrated in this work.

However, further research is needed before obtaining a robust computational tool with the accuracy required in real casting applications. First, although the viscoplastic compressible model[9,12,13] seems to be adequate to characterize the macroscopic mechanical behavior of the coherent solid phase in the mushy zone, this is contested by the lack of experimental (and literature) data in this range for determining the material parameters. Further, this model does not account for strain hardening, a mechanism that becomes important once the material is com-

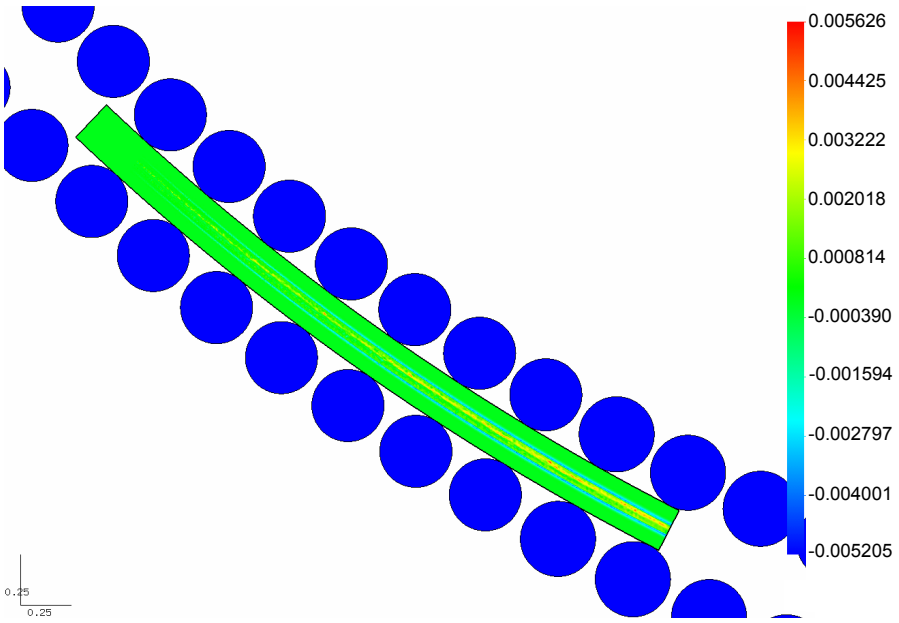

Figure 4: Final distribution of carbon segregation ($\langle w \rangle - w_0$) in the analyzed portion of the slab.

pletely solidified. Not only isotropic hardening must me modelled, as done by the "one-phase" models, but also kinematic hardening in order to account for alternate loading. The development of a library of constitutive models, suitable for one-phase and two-phase mechanical analysis, should be encouraged as future work.

Coupling between "one-phase" and two-phase analysis should be also improved when the first one is used to provide the second with initial conditions. In fact, being focused on the solidified shell, the "one-phase" solutions are quite inaccurate in the core of the strand, where the two-phase analysis is centered. However, this problem will be overcome once the two-phase analysis be operational on the whole casting domain.

A last remark concerns mesh discretization: a quite fine mesh is needed for an accurate description of the mushy zone. In the current version of R2SOL, the mesh is refined by regions defined a priori in the buffer zone. Then, as the solidification progresses and the width of the mushy zone decreases, there is an excessively fine mesh outside this zone. This suggests that the computational cost could be reduced by using adaptive remeshing, *i.e.*, by reducing the mesh size only where it is necessary. This is a work in progress.[24]

6 ACKNOWLEDGEMENTS

The financial support of ARCELOR Research, ASCOMETAL (from LUCCHINI group) and the French Ministère de l'Economie, des Finances et de l'Industrie, in the frame of the OSC-Continuous Casting project, is acknowledged. Victor D. Fachinotti is also granted by the Argentine Council for Scientific and Technical Research (CONICET).

REFERENCES

[1] M. C. Flemings. Our understanding of macrosegregation: past and present. *ISIJ International*, 40(9):833–841, 2000.

[2] C. Geindreau and J.-L. Auriault. Investigation of the viscoplastic behaviour of alloys in the semi-solid state by homogenization. *Mechanics of Materials*, 31:535–551, 1999.

[3] M. Hassanizadeh and W. G. Gray. General conservation equations for multi-phase systems: 1. averaging procedure. *Adv. in Water Resources*, 2:131–144, 1979.

[4] J. Ni and C. Beckermann. A volume-averaged two-phase model for transport phenomena during solidification. *Metall. Trans. B*, 22:349–361, 1991.

[5] C. Y. Wang and C. Beckermann. Equiaxed dendritic solidification with convection: Part 1. multiscale/multiphase modeling. *Metall. and Mat. Trans. A*, 27:2754–2764, 1996.

[6] M. Rappaz, M. Bellet, and M. Deville. *Numerical modelling in materials science and engineering*. Springer Verlag, New York, 2003.

[7] J.-L. Auriault and E. Sanchez-Palencia. Etude du comportement macroscopique d'un milieu poreux saturé déformable. *J. de Mécanique*, 16:575–603, 1977.

[8] S. Ganesan and D. R. Poirier. Conservation of mass and momentum for the flow of interdendritic liquid during solidification. *Metall. Trans. B*, 21:173–181, 1990.

[9] M. Abouaf, J.-L. Chenot, G. Raisson, and P. Bauduin. Finite element simulation of hot isostatic pressing of metal powders. *Int. J. Numer. Methods Engrg.*, 25:191–212, 1988.

[10] C. Geindreau, D. Bouvard, and P. Doremus. Constitutive behaviour of metal powder during hot forming. Part I: Experimental investigation with lead powder as a simulation material. *Eur. J. Mech. A/Solids*, 18:581–596, 1999.

[11] C. Geindreau, D. Bouvard, and P. Doremus. Constitutive behaviour of metal powder during hot forming. Part II: Unified viscoplastic modeling. *Eur. J. Mech. A/Solids*, 18:597–615, 1999.

[12] T. G. Nguyen, D. Favier, and M. Suery. Theoretical and experimental study of the isothermal mechanical behaviour of alloys in the semi-solid state. *Int. J. Plasticity*, 10:663–693, 1994.

[13] C. L. Martin, D. Favier, and M. Suéry. Viscoplastic behaviour of porous metallic materials saturated with liquid. part i: Constitutive equations. *Int. J. Plasticity*, 13(3):215–235, 1997.

[14] C. L. Martin, D. Favier, and M. Suéry. Viscoplastic behaviour of porous metallic materials saturated with liquid. part ii: Experimental identification on a Sn-Pb model alloy. *Int. J. Plasticity*, 13(3):237–259, 1997.

[15] C. L. Martin, D. Favier, and M. Suéry. Fracture behaviour in tension of viscoplatic porous metallic materials saturated with liquid. *Int. J. Plasticity*, 15:981–1008, 1999.

[16] C. Beckermann and J. Ni. Simulations of sedimentation in globulitic alloy solidification. *Int. Comm. Heat Mass Transfer*, 23(3):315–324, 1996.

[17] V. D. Fachinotti, S. Le Corre, N. Triolet, M. Bobadilla, and M. Bellet. Two-phase thermomechanical and macrosegregation modelling of binary alloys solidification with emphasis on the secondary cooling stage of steel slab continuous casting processes. Sent to Int. J.

Numer. Methods Engrg., 2005.

[18] E. Perchat, L. Fourment, and T. Coupez. Mixed formulation and iterative solver for the parallelisation of a forging simulation software by mesh partitioning. In B. H. V. Topping, editor, *3rd Euro Conf. on Parallel and Distributed Computing for Computational Mechanics*, pages 67–72, Weimar, Germany, 1999.

[19] M. Bellet and V. D. Fachinotti. ALE method for solidification modeling. *Comput. Methods Appl. Mech. Engrg.*, 193:4355–4381, 2004.

[20] A. N. Brooks and T. J. R. Hughes. Streamline upwind/Petrov-Galerkin formulations for convection dominated flows with particular emphasis on the incompressible Navier-Stokes equations. *Comput. Methods Appl. Mech. Engrg.*, 32:199–259, 1982.

[21] P. F. Kozlowski, B. G. Thomas, J. A. Azzi, and H. Wang. Simple constitutive equations for steel at high temperature. *Metall. and Mat. Trans. A*, 23:903–918, 1992.

[22] A. Heinrich. *Modélisation thermomécanique de la coulée continue d'acier en deux dimensions*. PhD thesis, Ecole des Mines de Paris, France, 2003.

[23] M. Bellet and A. Heinrich. A two-dimensional finite element thermomechanical approach to a global stress-strain analysis of steel continuous casting. *ISIJ Int.*, 44(10):1686–1695, 2004.

[24] W. Liu. *Finite element modelling of macrosegregation and thermomechanical phenomena in solidification processes*. PhD thesis, Ecole des Mines de Paris, France, 2005.

[25] M. Reza Aboutalebi, M. Hasan, and R. I. L. Guthrie. Coupled turbulent flow, heat, and solute transport in continuous casting processes. *Metall. and Mat. Trans. B*, 26:731–744, 1995.